IDF curves for future climate scenarios in a locality of the Tapajós Basin, Amazon, Brazil

Carlos Eduardo Aguiar de Souza Costa, Claudio José Cavalcante Blanco and José Francisco de Oliveira-Júnior

ABSTRACT

Changes in the global climate are attributed to the levels of greenhouse gases. Thus, future scenarios (Representative Concentration Pathways – RCPs) have been developed to explore the impact of different climate policies on the world. The RCPs are essential tools for General Circulation Models (GCMs) to simulate future climate changes. Curves that associate Intensity, Duration and Frequency (IDF) are used in forecasts and are fundamental for the design of hydraulic projects and risk management. The objective of this study was to design IDF curves for the RCP 4.5 and 8.5, using data from the HadGEM2-ES, CanESM2 and MIROC5 models. The Equidistance Quantile Matching Method was used to design the IDF curves. The simulated curves presented differences when related to the existing curve. The largest differences were for the MIROC5 (146% in RCP 8.5) and the smallest differences were for the CanESM2 (−20.83% for RCP 8.5). This result demonstrates that the method incorporates changes in future climate variability. The spatial resolutions of each model influenced their IDF curves, which led the CanESM2 curves to not present satisfactory results that are different from the MIROC5 curves, which were the ones that best represented the possible future differences.

Key words | climate change, hydraulic projects, risk management

Carlos Eduardo Aguiar de Souza Costa
Claudio José Cavalcante Blanco (corresponding author)
Graduate Program in Civil Engineering (PPGEC),
Federal University of Pará (UFPA),
66075-110, Belém, Pará,
Brazil
E-mail: *blanco@ufpa.br*

José Francisco de Oliveira-Júnior
Institute of Atmospheric Sciences (ICAT),
Federal University of Alagoas (UFAL),
57072-260, Maceió, Alagoas,
Brazil

INTRODUCTION

With the understanding that climate change is unavoidable, global climate policy has shifted its focus on mitigation to preparedness and adaptation to future impacts (Porter *et al.* 2015). Faced with these concerns, the World Meteorological Organization (WMO) and the United Nations Environment Program (UNEP) have created the Intergovernmental Panel on Climate Change (IPCC). This body regularly brings together several climate research centers around the world to update climate models, prepare technical reports and other products on possible scenarios of greenhouse gas emissions and the impacts on the different climate scopes (Pachauri & Meyer 2014).

The fifth IPCC report (AR5), adopted in 2014, indicates that temperature rise is especially attributable to greenhouse gas levels. Most of the time, the greenhouse effect is linked to development. From this, there was interest from governments in scenarios that better explore the impact of different climate policies, analyzing the 'cost–benefit' of long-term climate objectives. In response, the IPCC asked the scientific communities to develop a set of scenarios that would replace the old ones (called Special Report Emission Scenarios – SRES) created during the fourth report and facilitate the assessment of future situations. The RCPs (Representative Concentration Pathways) scenarios were proposed, and those most used for the future simulations (2006–2100) are the RCP 2.6, RCP 4.5 and RCP 8.5. The RCP 2.6 scenario is the least likely scenario to occur, while RCP 4.5 is the desired scenario, wherein countries can control emission levels and the level of CO_2 in the atmosphere stabilizes soon after 2100. However, the RCP

doi: 10.2166/wcc.2019.202

8.5 scenario is recognized as more likely to occur (Schardong *et al.* 2014). The RCPs are essential pieces for the General Circulation Models (GCMs) because it is from them that these numerical models represent the future physical processes in the atmosphere, ocean and terrestrial surface. The GCMs are the most advanced tools available to simulate the response of the global climate system to increased concentrations of greenhouse gases. The outputs generated by models from different countries were assembled in the Coupled Model Intercomparison Project Phase 5 (CMIP5), a project designed during AR5 that succeeded CMIP3, which also aimed to facilitate access to these data. Silveira *et al.* (2013) analyzed the efficiency of some of these models in Brazil and concluded that the majority had high correlations with respect to the climatology observed in the Northeast, Prata Basin and Amazon regions, showing that they are able to capture patterns of seasonal variations, mainly precipitation.

The Amazon and the Northeast represent the country's most vulnerable regions to climate change. In the Amazon region, several extreme hydrological events have occurred in the last decades, such as the floods of 2009, 2012 and 2014, and the droughts of 2005 and 2010, which served as warnings about the impacts of climate variability (Marengo & Espinoza 2015). Therefore, it is important to evaluate intense precipitation in the past and future to analyze the impact of climate change on water resources. The characteristics of the intense rains, or curves that associate Intensity, Duration and Frequency (IDF), represent fundamental information for the design of hydraulic works, such as drainage systems, retention basins and dams. Most of the existing IDF curves have been elaborated on the theory of extreme stationary values; however, it is now widely recognized that climate change is creating a non-stationary component and intensifying these events (Agilan & Umamahesh 2016). Therefore, it is necessary to carefully examine the IDF curves and perform projections since their changes may pose great future risks to society. Although a few recent studies were performed in Brazil, none were done in the Amazon (Sabóia *et al.* 2017). Therefore, the objective of this study was to design IDF curves in the Tapajós catchment basin for future scenarios RCP 4.5 and 8.5. This is one of the main basins in the Amazon region, and it possesses strategic value for several projects planned in this region, such as hydroelectric plants, waterways, railroads and highways.

This paper is structured by starting the methodology obtaining the precipitation data and GCMs data for the defined region. Afterwards, the data of the climate models are read and analyzed to perform the downscaling and the temporal projection. In the Results section, the variation of the future precipitation and the historical period modeled by the three GCMs are discussed, then the IDF curves and the intense rain equations are presented and compared with the one existing in the region, considering a return period of 100 years. Finally, the work with the main results obtained by the study is concluded.

PRECIPITATION DATA AND AREA OF STUDY

The precipitation data used in this study have no flaws and were obtained together with the Second Meteorological District in the Institute of Meteorology (DISME-INMET). The historical series is 10 years (2008–2017), referring to station code 82191, registered with the WMO. The data were on an hourly scale and were organized in spreadsheet form. The mean annual rainfall was 1,630.26 mm and the monthly mean was 185.2 mm. The hourly mean was 0.23 mm (60 minutes) to 5.18 mm (1,440 minutes), with a standard deviation (SD) ranging from 1.78 to 12.81 mm. The maxima were obtained by separating the specific time intervals (Table 1).

Note that the GCMs data were read through the Ferret tool (NOAA 2018) to the same point at which the station is located (04°16′37.12″S and 55°59′35.11″W), that is, located near the Tapajós River. The catchment area of the Tapajós basin (Figure 1) is one of the basins that have the greatest electricity generation potential in Brazil, with an area of 764,183 km², which is almost the size of Sweden and Norway combined (Fearnside 2015). The area is strongly influenced by the ENSO phenomenon. The main atmospheric system operating in the region is the Intertropical Convergence Zone (ITCZ), which also presents low pressure, being a characteristic of regions close to the Equator.

Next to the study point is the construction of the São Luiz do Tapajós hydroelectric plant. It will be the fourth

Table 1 | Precipitation data maximum rainfall organized, mean and standard deviation of the general data

Maximum (mm)

Years	60 min.	120 min.	240 min.	360 min.	720 min.	1,080 min.	1,440 min.
2008	90.80	103.20	112.6	116.80	120.20	120.20	120.20
2009	43.60	72.20	78	81	81.40	97.40	98.20
2010	66.40	83.20	85.2	88.80	100	100	104.20
2011	59.40	73.40	86	105	109.60	110.40	110.40
2012	39	55.20	60.6	71.60	91	102	102
2013	73.20	103.60	110.4	111.80	113.80	127.20	127.80
2014	65.20	90	93.2	94.60	94.60	109.20	116
2015	44.80	50.80	56	61	80	81.20	81.20
2016	42.80	57.40	63	69.80	71	71	72.60
2017	53.80	59.80	82	89	105.20	106	106.40
Mean	57.90	74.88	82.70	88.94	96.68	102.46	103.90
SD	16.41	19.53	19.44	18.56	16.00	16.74	16.88

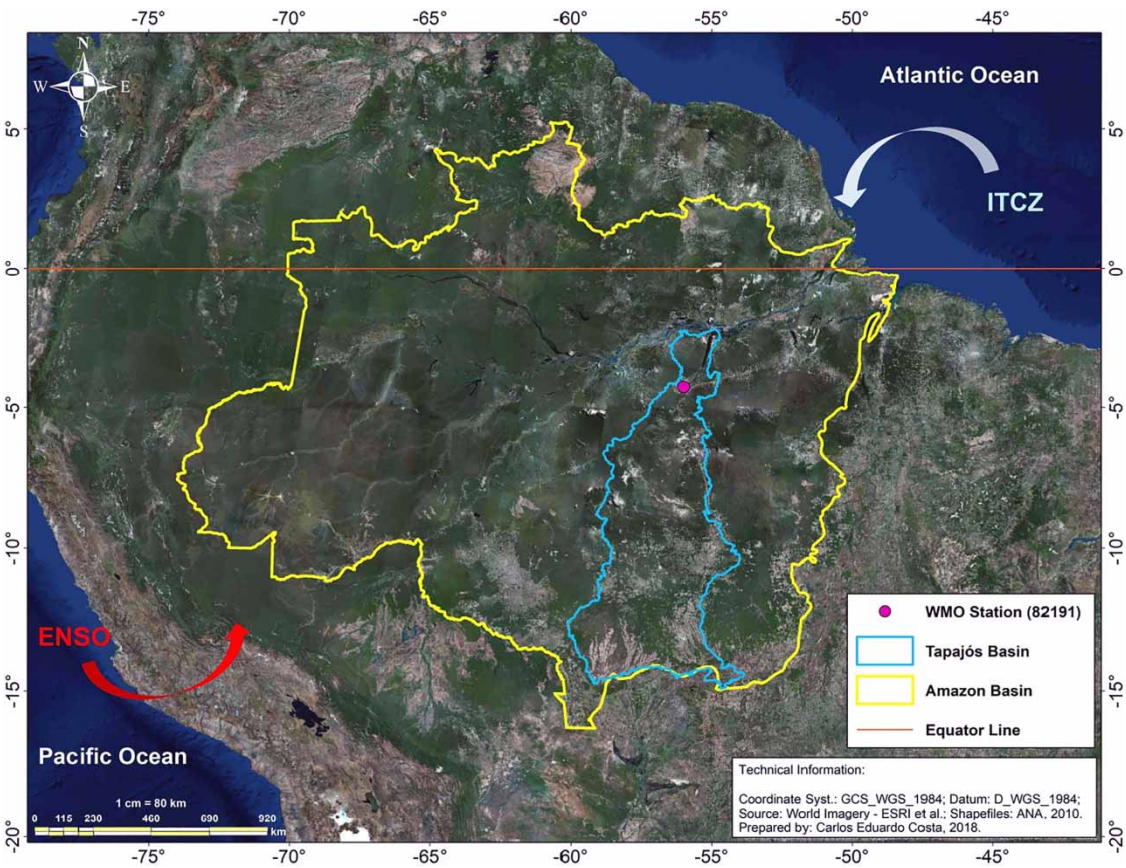

Figure 1 | Region of study.

largest hydroelectric plant in the country, with a capacity of 8,040 MW. In the Tapajós basin, there are a large number of dams; by 2022, there will be more than 40 projects, including ports, small hydroelectric plants and large hydropower plants. The chosen study point is also strategic for roads, since the site gives access to the two main highways of the Amazon, namely BR-163 and BR-230 (Trans-Amazonian). Completion of planned works for these highways will also provide a shift in agricultural production, which should accelerate development and occupation in the area. There is also a planned railroad, called 'Ferrogrão,' with authorization for a project feasibility study that will transport approximately 40% of grain and bran production in this region (Walker & Simmons 2018).

METHODS

GCMs data

Research centers around the world have made CMIP5 data available via the World Climate Research Program (https://esgf-node.llnl.gov) in the Network Common Data Format (NetCDF). In this site, the outputs of the GCMs can be found for 725 climatic variables (precipitation, wind, radiation, and SO_2 concentration, among others) for all RCPs scenarios and historical simulations. The historical experiment serves as a basis for the future scenarios of each GCM (2006–2100) since it is aligned in natural and anthropogenic atmospheric changes observed between 1850 and 2005.

The data use the nomenclature 'r_i_p_' in the configuration of the simulations performed. The 'r' equals the number of realizations; 'i' means the different initiations with physical implications and the 'p' are the perturbations in physics for each of the simulated models (Silveira *et al.* 2013). Currently, 45 models are available for the r1i1p1 set of historical simulations. The number of models available for RCP 2.6, 4.5, and 8.5 with the r1i1p1 set are 27, 43 and 41, respectively.

Some models offer outputs with more than one initial condition (r1i1p1, r2i1p1 and r3i1p1). However, in this work, only daily precipitation data with the initial configuration r1i1p1, due to their greater availability and ability to maintain the initial conditions of the GCMs, were chosen. Only the RCP 4.5 and RCP 8.5 scenarios were considered for three reasons: (1) they are the main representatives of optimistic and realistic scenarios in the future; (2) they are the most used in scientific studies; and (3) the occurrence of the RCP 2.6 scenario is almost unlikely. Work with IDF curves projections can be performed with various amounts of GCMs for analysis, from one GCM as in the work of Srivastav *et al.* (2014a), up to 24 models as in Agilan & Umamahesh (2016). In this work we opted for the choice of three GCMs to optimize the search time and to maintain an acceptable quantity for a minimally consistent analysis. The three GCMs most commonly used in climatic studies in the Amazon (Negrón-Juárez *et al.* 2015; Villamayor *et al.* 2018) were chosen, and Table 2 provides details of these models.

Studies using several models are necessary to verify the possible uncertainties in the future scenarios, since each model has its advantages and disadvantages. The HadGEM2 model with Earth System (ES) coupling is the best among the three to understand the contributions of biogeochemical feedback to the evolution of the global climate system, since it does not require corrections of atmospheric fluxes. The Japanese MIROC5 model was developed for the

Table 2 | Details of the GCMs used in the study

Model	Full Name	Country	Institution	Atmospheric Grid (Long. × Lat.)
CanESM2	Canadian Earth System Model Version 2	Canada	Canadian Climate Center for Modelling and Analysis	2.8 × 2.8°
HadGEM2-ES	Hadley Centre Global Environmental Model Version 2 – Earth System	United Kingdom	Met Office Hadley Centre	1.875 × 1.25°
MIROC5	Model for Interdisciplinary Research on Climate Version 5	Japan	Center for Climate System Research	1.4 × 1.4°

better simulation of climatic variability influenced by phenomena. This model simulates the *El Niño*-Southern Oscillation (ENSO) more realistically than others and efficiently designs climatological precipitation, especially for the ITCZ area of influence (Watanabe *et al.* 2010). The results derived from CanESM2 are robust; however, several results demonstrate that it overestimates the response to greenhouse gases, and its internal climatic variability is lower than those of other models (Gillett *et al.* 2012).

GCMs precipitation data reading and analysis

The reading was performed through the Ferret grid data analysis tool, installed on the Linux operating system, Ubuntu 16.04 LTS. This software was developed by the Thermal Modelling and Analysis Project (TMAP) of the Pacific Marine Environmental Laboratory (PMEL/NOAA), in Seattle, USA, with the objective of analyzing the results of its numerical ocean models and comparing them with observational grid data (Ohunakin *et al.* 2015). The data sets of the models are generally many gigabytes in size, with mixed variables of three and four dimensions defined in stepwise networks. The features that make Ferret different from other programs are its mathematical flexibility, geophysical formatting, intelligent 'connection' to its database, and memory management for very large calculations (NOAA 2018).

Downscaling and temporal projection

Due to the lack of sufficient spatial resolution, the GCMs results need to be post-processed before their use. Dynamic or statistical downscaling methods are necessary to remove systematic deviations in models and to transform simulated climatic patterns to a more refined spatial resolution of local interest (Sachindra *et al.* 2014). The intensive computational nature makes it difficult to use dynamic downscaling because it uses high-resolution models to simulate physical processes. In contrast, numerous studies have shown that the performance of statistical downscaling can be similar to that of dynamic downscaling since they are computationally accessible and transform larger-scale climate projections on a more precise scale through statistical functions (Wang *et al.* 2016).

Li *et al.* (2010) proposed a simple statistical downscaling methodology, a bias correction method called Equidistance Quantile Matching Method, which has the advantage of explicitly incorporating changes in future climate variability by relating the cumulative distribution functions between the variables. Based on this method, Srivastav *et al.* (2014a) developed an algorithm to be applied in the IDF curve update procedure. This algorithm was incorporated into a Canadian Water Network project, called 'IDF_CC Tool', a web tool accessible to all interested in the development of IDF curves that considers the projected impacts of climate change (Simonovic *et al.* 2016). This tool includes a set of mathematical procedures: (1) statistical analysis algorithms; (2) an optimization algorithm; (3) a GCM selection algorithm; and (4) an IDF update algorithm. The last algorithm, provided by Srivastav *et al.* (2014b), was handled and adapted through the MATLAB language with the needs and data available for this study. Figure 2 shows the schematization of the algorithm.

Schardong *et al.* (2018) commented that the Gumbel distribution has been widely recommended for hydrological studies and was adopted as the standard by the Environment and Climate Change Canada (ECCC), which also suggests using the moments method in the statistical procedure to estimate distribution parameters. The amount of sub-daily data used to calculate the IDF curves should be 10 years or more, and this value is also stipulated by the ECCC (Schardong *et al.* 2018). Thus, it was used as a basis for correction of 10 years (2008–2017) bias of hourly data, with the input being the maximums of 60, 120, 240, 360, 720, 1,080 and 1,440 minutes. Data for the historical maximums of the GCMs were 30 years (1976–2005) and the future maximums for GCMs were 95 years (2006–2100), such as those used by Srivastav *et al.* (2014b), as well as the return periods of 2, 5, 10, 25, 50 and 100 years.

The three main steps involved in using the algorithm are: (1) Spatial downscaling: establishing statistical relationships between the maximum daily GCM historical data and each of the sub-daily maximums observed at the station of interest using quantum mapping functions; (2) Temporal downscaling: establishing statistical relationships between the maximums of the historical period of the GCM and the future period using quantile mapping functions; and (3) Establishing statistical relationships between steps (1) and (2) to update the IDF curves for future periods.

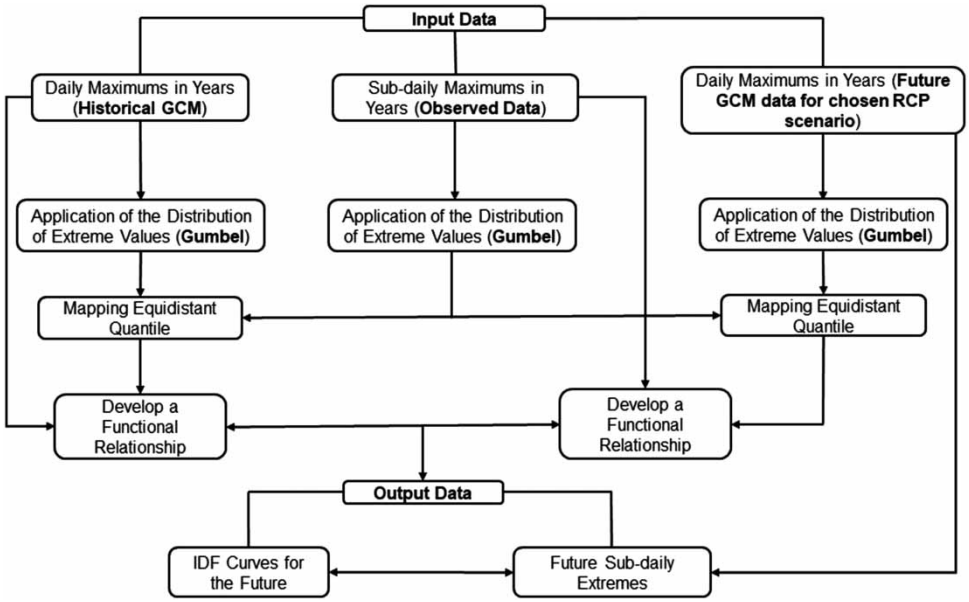

Figure 2 | Schematization of the algorithm for generation of future IDF curves adapted from Srivastav *et al.* (2014b).

Intense rainfall equations

Sherman (1931) established a mathematical relation that expresses the IDF curves and is currently the one that is most used (Equation (1)):

$$I = \frac{a.\ Tr^b}{(t+c)^d} \tag{1}$$

where I is the intensity of rain (mm/h); Tr is the return period (years); t is the duration (minutes); and a, b, c, e and d are specific constants to each locality. For the calculation of the constant 'c', we use the method mentioned by Sabóia *et al.* (2017), in which within the N years of data used in the study, extreme events occur every five years. Thus, the 95 years used for the projections for five years were divided, and the result was closer to the Tr of 25 years, which was chosen; then we defined the parameter 'A' (Equation (2)):

$$I = \frac{A}{(t+c)^d} \tag{2}$$

An anamorphosis was then performed, linearizing the data through a bilogarithmic graph between I and t for the Tr defined in the previous method. In this graph, the points (I_1, t_1) and (I_2, t_2) were designated the start and end points of the curve, respectively. Also determined from this curve was the point I_3 through Equation (3) and t_3 using the equation generated in the graph by the potency relationship, which was the one that best fit the data:

$$I_3 = \sqrt{I_1.\ I_2} \tag{3}$$

From this, the constant 'c' can be obtained by Equation (4):

$$c = \frac{t_3^2 - t_1.\ t_2}{t_1 + t_2 - 2.\ t_3} \tag{4}$$

Afterwards, a bilogarithmic plot of the intensities of the chosen Tr as a function of the displacements by the constant c (t+ c), for the determination of the constants 'A' and 'd', was plotted again. It was verified that the best fit to the points is again of potency, generating Equation (5), with the constant 'd':

$$I = A\ .(t+c)^{-d} \tag{5}$$

Note that Equation (5) directly provides values of parameter 'A' and constant 'd'. However, the value of the

constant '*d*' that is used will be the one generated for the chosen *Tr*, while the constant '*A*' will vary to obtain the constants '*a*' and '*b*'. For each *Tr*, a graph similar to the previous one was created, which provided new values for parameter '*A*'. Again, a bilogarithmic graph was created between the values of '*A*' obtained and all *Tr* values. Thus, after adjusting the potency relationship, Equation (6) was generated, in which the values of the constants '*a*' and '*b*' can be found:

$$A = a \cdot Tr^{b} \quad (6)$$

RESULTS AND DISCUSSION

Precipitation variability based on GCMs

Before the elaboration of the IDF curves, a previous analysis of the data generated by the GCMs models was carried out to verify the possible changes in the pluviometric regime in the next 100 years. The mean of the maximum daily precipitation and annual precipitation data were compared between their respective historical bases and their future projections. For this, the periods from 1976 to 2000 and from 2076 to 2100 for all models were chosen for the two chosen RCPs scenarios. In Figure 3, the graph shows the variations of mean maximum precipitation per day.

The MIROC5 model presented the highest variation for CPR 8.5 (50.22%), almost four times higher than that for the RCP scenario 4.5 (13.41%). For the HadGEM2-ES model, scenario 8.5 also presented a greater variability (20.94%) when compared to the other scenario (1.56%). This demonstrates that in the most realistic scenario, rainfall maximums will increase, as Agilan & Umamahesh (2016) commented in their study, providing a warning such that the concern in the design of works of water resources engineering has been intensified. The CanESM2 model was the one that differed from the others, since in its two scenarios it showed a decrease in its variation. In RCP 4.5, this variation was −15.07%, and in RCP 8.5, it was −8.46%. These values may be related to the decrease in precipitated annual volumes, as can be observed in Figure 4.

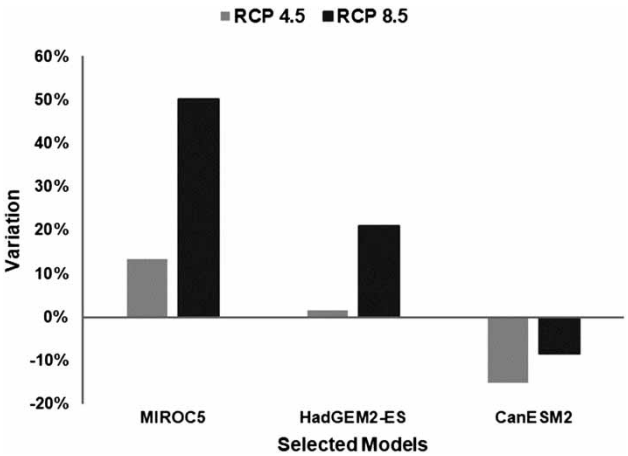

Figure 3 | Variation in mean maximum daily intensities from 2076 to 2100 based on the GCMs historical data (1976–2000).

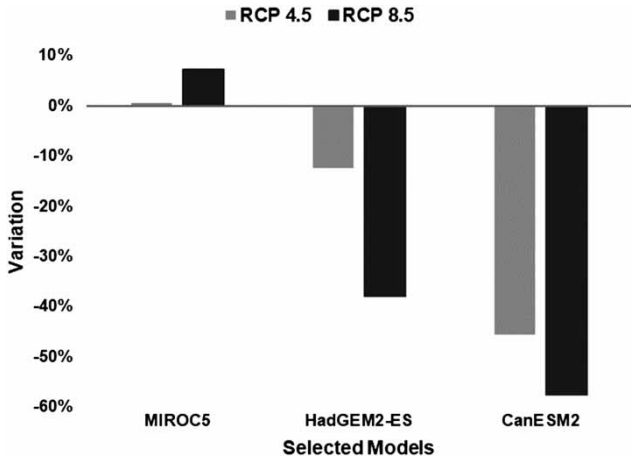

Figure 4 | Variation in mean annual total precipitation from 2076 to 2100 based on GCMs historical data (1976–2000).

It is noteworthy that in several studies, such as Pachauri & Meyer (2014), the total precipitation will decrease in most of the results of the CMIP5 models for both the RCP 4.5 scenario and the RCP 8.5 scenario. In the latter scenario, the decrease will be even more severe, as seen by analyzing Figure 5. The CanESM2 model showed an alarming decrease for both scenarios, more than half (−57.64%) for RCP 8.5 and −45%, and 74% for the other scenario, RCP 4.5. The values were also significant in HadGEM2-ES projections (RCP 8.5 was −37.89% and RCP 4.5 was −12.37%). The MIROC5 model did not show any decrease in precipitation; however, its increase data were not relevant: 0.52% for RCP 4.5 and 7.29% for RCP 8.5.

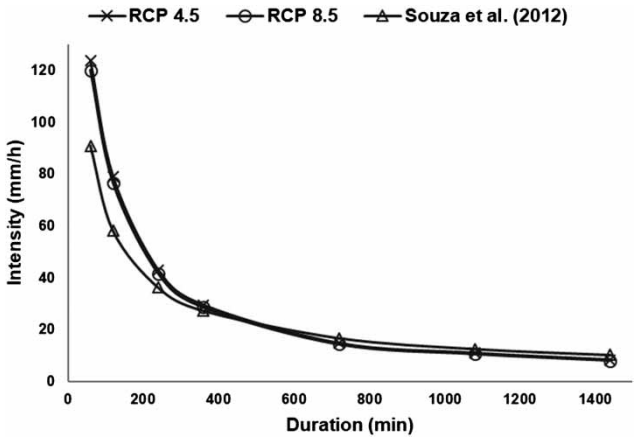

Figure 5 | Comparison between the IDF curves designed for RCP 4.5 and RCP 8.5 of the CanESM2 model and Souza *et al.* (2012) for the *Tr* of 100 years.

Projected IDF curves and their equations

For a better analysis, the projected IDF curves were compared with that obtained by Souza *et al.* (2012) for the same point of study. The authors developed intense rain equations for several stations with historical data of at least 10 years. The curve developed by the authors was called 'Souza *et al.*', to facilitate discussion. Table 3 shows the equation of Souza *et al.* and those projected for the future scenarios, together with their respective values of fit with respect to the curves. It is worth mentioning that the *Tr* value of 100 years was used to generate the IDF curves of the comparison, which is important for precisely explaining possible changes in precipitation patterns caused by future climate changes.

In the IDF curves generated for the CanESM2 model (Figure 5), there is a close relationship between the curves for the two scenarios, which shows little variation between the intensities. When compared to that of Souza *et al.*, a difference of approximately 30% in the two was observed until approximately 240 minutes, when the curves began to overlap. For this model, the differences were not high between the two scenarios; the highest was RCP 4.5 with 36.24%, but it was close to 32% for RCP 8.5. For the duration of 1,440 minutes, or 1 day, the curves underestimated the values of Souza *et al.*, presenting a mean difference of −20%.

It is expected that, when compared, the curves for future scenarios have values different from those obtained by Souza *et al.* since the authors used historical data (the last 30 years until 2012) to create curves for the present day. It should be pointed out that the authors used a method considered a stationary method (the relations method) to obtain these curves, which further reaffirms the fact that the projected curves by this study (with reach up to 2100) will possibly have different values. The differences observed in Figure 5 may also mean that this model is not efficient for this type of methodology. This corroborates the results of Sabóia *et al.* (2017), who observed the low spatial resolution of the CanESM2 model, that is, $2.8 \times 2.8^{\circ}$ (longitude × latitude). This detail may be responsible for this inefficiency, which, according to Cheng & Aghakouchak (2014), is dangerous because designing systems based on projections that do not represent the reality of climate change may not be enough to mitigate future impacts on the population.

Table 3 | Equations for new scenarios and the coefficient R^2 for the adjustments

Equations – IDF curves				
Souza *et al.* (2012)	$I = \frac{1073.27.\ Tr^{0.1317}}{(t+9.785)^{0.7242}}$		$R^2 = 0.9939$	
Models	**RCP 4.5**	**R^2**	**RCP 8.5**	**R^2**
MIROC5	$I = \frac{3583.2.\ Tr^{0.267}}{(t+13.335)^{0.936}}$	0.9955	$I = \frac{4087.4.\ Tr^{0.284}}{(t+13.45)^{0.943}}$	0.9954
HagGEM2-ES	$I = \frac{2350.\ Tr^{0.177}}{(t+14.385)^{0.905}}$	0.9967	$I = \frac{2516.6.\ Tr^{0.242}}{(t+14.379)^{0.920}}$	0.9964
CanESM2	$I = \frac{2038.\ Tr^{0.294}}{(t+14.773)^{0.919}}$	0.9965	$I = \frac{2012.3.\ Tr^{0.283}}{(t+14)^{0.915}}$	0.9964

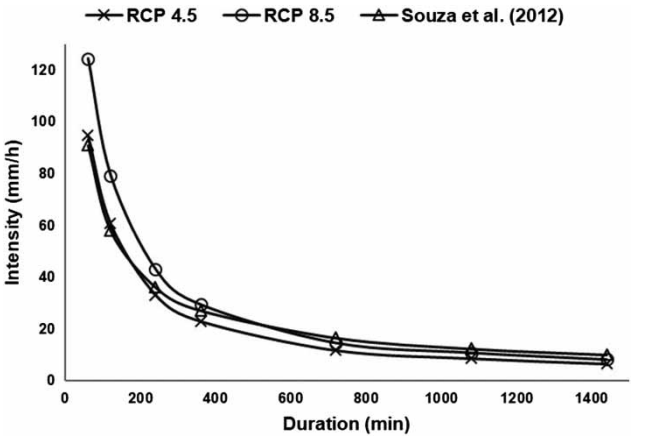

Figure 6 | Comparison between the IDF curves designed for the PCR 4.5 and RCP 8.5 of HadGEM2-ES and Souza *et al.* (2012) for the *Tr* of 100 years.

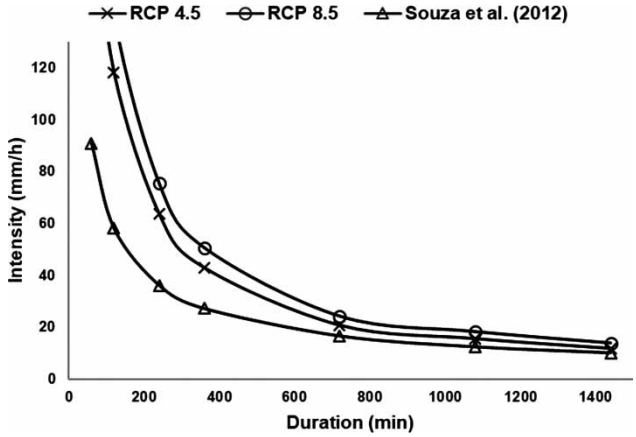

Figure 7 | Comparison between the IDF curves projected for RCP 4.5 and RCP 8.5 of the MIROC5 model and Souza *et al.* (2012) for the *Tr* of 100 years.

The next analysis was performed with the HadGEM2-ES model (Figure 6), in which it is observed that the scenarios presented values slightly more different from each other. In the RCP 4.5 scenario, the intensities remained above the curve defined by Souza *et al.* until approximately 180 minutes, with an approximately 4% difference, when it began to present values below, reaching up to −35%. In the RCP 8.5 scenario, initially the projected curves and that of Souza *et al.* presented a greater distance, with a difference of approximately 35% between them. The projected curve remained higher than that of Souza *et al.* up to slightly more than 400 minutes, when it began to decrease, reaching the end below the curve mentioned, with a difference of 18.35% between the two curves.

It can be said that the HadGEM2-ES model presented reasonable results for the IDF curves, but some values continued to overlap and to be very close to the curve of Souza *et al.* Statistical downscaling may not have been sufficient to refine the data and obtain more satisfactory results, which, in turn, could be easily obtained if the model underwent dynamic downscaling. This is noticeable in the work of Liew *et al.* (2014), who used a more refined regional model to generate the curves, called WRF/ERA40, and obtained better results in the projection of the IDF curves.

The MIROC5 model presented the best results. Figure 7 shows that the highest intensities were for RCP 8.5, which, when compared to the curve of Souza *et al.*, showed a difference of 143% for 60 minutes, and then decreased up to 37% in 1,440 minutes. The RCP 4.5 remained at lower intensities than the other scenario; however, they also remained above the Souza *et al.* curve, with differences from 104% (60 minutes) to 17% (1,440 minutes).

These results contribute to reaffirm the research of Alemseged & Tom (2015). The authors performed an analysis of climatic variables in Ethiopia (area under the influence of the ITCZ) using these three models and concluded that MIROC5 is superior to the other models in relation to capturing precipitation anomalies. Sabóia *et al.* (2017) stated that among the other GCMs models used in this study, this is the one with the best spatial resolution.

CONCLUSIONS

The variability in the GCMs projections up to 2100 mostly showed a decrease in the annual precipitation on the CanESM2 and HadGEM-ES models, and an increase in the model MIROC5. The variations predict an increase in the maximum daily rainfall intensities for the MIROC5 and HadGEM2-ES models and decrease for the CanESM2. The rainfall equations generated for the climatic scenarios presented satisfactory adjustment coefficients (all above 0.99), demonstrating that they are effective tools for the possible design of water works and future risk management.

The Equidistant Quantile Matching Method was shown to be effective and could be easily applied with low computational resources. The simulated IDF curves showed differences when related to the already existing curve for

the study point, which may indicate that the method actually incorporates explicit changes in the future climate variability. This reaffirms the hypothesis of greater efficiency of a method that takes into account the non-stationarity of climatic variables.

Even with the GCMs having a 'coarser' grid, statistical downscaling was able to distinguish changes in intensities between time periods. However, the spatial resolutions of each model strongly influenced their IDF curves, which led the CanESM2 curves to not present satisfactory results with respect to the curves created from the work of Souza *et al.* (2012), unlike the MIROC5 curves, which represented the best possible differences in future precipitation. These facts suggest that in the future, this methodology can be reapplied with more refined models or regional climate models, as these have better spatial and temporal resolutions.

ACKNOWLEDGEMENTS

The authors would like to thank ANA and INMET for kindly providing rainfall data for current analysis. The first author would like to thank CAPES for the PhD's degree scholarship. The second author would like to thank CNPq for funding the research productivity grant (Process 304936/2015-4). The third author would like to thank CNPq for the research productivity grant (Process 306410/2015-0).

REFERENCES

Agilan, V. & Umamahesh, N. V. 2016 Is the covariate based non-stationary rainfall IDF curve capable of encompassing future rainfall changes? *J. Hydrol.* **541**, 1441–1455.

Alemseged, T. H. & Tom, R. 2015 Evaluation of regional climate model simulations of rainfall over the Upper Blue Nile basin. *Atmos. Res.* **161**, 57–64.

Cheng, L. & Aghakouchak, A. 2014 Nonstationary precipitation intensity-duration-frequency curves for infrastructure design in a changing climate. *Sci. Rep.* **4**, 7093.

Fearnside, P. M. 2015 Amazon dams and waterways: Brazil's Tapajós Basin plans. *Ambio* **44** (5), 426–439.

Gillett, N. P., Arora, V. K., Flato, G. M., Scinocca, J. F. & Salzen, K. V. 2012 Improved constraints on 21st-century warming derived using 160 years of temperature observations. *Geophys. Res. Lett.* **39** (1), 1–5.

Li, H., Sheffield, J. & Wood, E. F. 2010 Bias correction of monthly precipitation and temperature fields from Intergovernmental Panel on Climate Change AR4 models using equidistant quantile matching. *J. Geophys. Res. Atmos.* **115** (D10), 1–20.

Liew, S. C., Raghavan, S. V. & Liong, S. 2014 How to construct future IDF curves, under changing climate, for sites with scarce rainfall records? *Hydrol. Process.* **28** (8), 3276–3287.

Marengo, J. A. & Espinoza, J. C. 2015 Extreme seasonal droughts and floods in Amazonia: causes, trends and impacts. *Int. J. Climatol.* **36** (3), 1033–1050.

Negrón-Juárez, R. I., Koven, C. D., Riley, W. J., Knox, R. G. & Chambers, J. Q. 2015 Observed allocations of productivity and biomass, and turnover times in tropical forests are not accurately represented in CMIP5 Earth system models. *Environ. Res. Lett.* **10** (6), 064017.

NOAA – National Oceanic and Atmospheric Administration 2018 *Data Visualization and Analysis*. Available from: http://ferret.pmel.noaa.gov/Ferret/ (accessed 28 may 2018).

Ohunakin, O. S., Adaramola, M. S., Oyewola, O. M., Matthew, O. J. & Fagbenle, R. O. 2015 The effect of climate change on solar radiation in Nigeria. *Solar Energy* **116**, 272–286.

Pachauri, R. K. & Meyer, L. A. 2014 *Climate Change 2014: Synthesis Report*. Contribution of Working Groups I, II and III to the fifth assessment report of the Intergovernmental Panel on Climate Change. IPCC, Geneva, Switzerland, p. 151.

Porter, J. J., Demeritt, D. & Dessai, S. 2015 The right stuff? Informing adaptation to climate change in British local government. *Glob. Environ. Change* **35**, 411–422.

Sabóia, M. A. M. D., Souza Filho, F. A., Araújo Júnior, L. M. D. & Silveira, C. S. 2017 Climate changes impact estimation on urban drainage system located in low latitudes districts: a study case in Fortaleza-CE. *Rev. Bras. Recur. Hídr.* **22**, e21.

Sachindra, D. A., Huang, F., Barton, A. & Perera, B. J. C. 2014 Statistical downscaling of general circulation model outputs to catchment scale hydroclimatic variables: issues, challenges and possible solutions. *J. Water Clim. Change* **5** (4), 496–525.

Schardong, A., Simonovic, S. P. & Garcia, J. I. B. 2014 O possível efeito de mudanças climáticas e suas incertezas sobre afluências em sistemas de recursos hídricos (The possible effect of climate change and its uncertainties on inflows in water resources systems). *Rev. Gest. Água Am. Lat.* **11** (2), 53–65.

Schardong, A., Gaur, A., Simonovic, S. P. & Sandink, D. 2018 *Computerized Tool for the Development of Intensity-Duration-Frequency Curves Under A Changing Climate*. Technical Manual 3.0. Western University, Canada.

Sherman, C. W. 1931 Frequency and intensity of excessive rainfalls at Boston. *Massachusetts. Trans. Am. Soc. Civil Eng.* **95** (1), 951–960.

Silveira, C. S., Souza Filho, F. A., Costa, A. A. & Cabral, S. L. 2013 Performance evaluation of the CMIP5 models regarding the representation of rainfall variation patterns in the twentieth

century over the Northeast region of Brazil, the Amazon and the Prata Basin and analysis of the projections for the scenario RCP 8.5 (in Portuguese). *Rev. Bras. Meteorol.* **28** (3), 317–330.

Simonovic, S. P., Schardong, A., Sandink, D. & Srivastav, R. 2016 A web-based tool for the development of intensity duration frequency curves under changing climate. *Environ. Model. Softw.* **81**, 136–153.

Souza, R. O. D. M., Scaramussa, P. H., Amaral, M. A., Pereira Neto, J. A., Pantoja, A. V. & Sadeck, L. W. 2012 Equações de chuvas intensas para o Estado do Pará (Equations of intense rainfalls for the State of Pará). *Rev. Bras. Eng. Agr. Ambient.* **16** (9), 999–1005.

Srivastav, R. K., Schardong, A. & Simonovic, S. P. 2014a Equidistance quantile matching method for updating IDF Curves under climate change. *Water Resour. Manage.* **28** (9), 2539–2562.

Srivastav, R. K., Schardong, A. & Simonovic, S. P. 2014b *Computerized Tool for the Development of Intensity-Duration-Frequency Curves Under A Changing Climate*. Technical Manual 1. Western University, Canada.

Villamayor, J., Ambrizzi, T. & Mohino, E. 2018 Influence of decadal sea surface temperature variability on northern Brazil rainfall in CMIP5 simulations. *Clim. Dyn.* **51** (1–2), 563–579.

Walker, R. & Simmons, C. 2018 Endangered Amazon: an indigenous tribe fights back against hydropower development in the Tapajós Valley. *Environ. Sci. Pol. Sustain. Dev.* **60** (2), 4–15.

Wang, L., Ranasinghe, R. W. M. R. J., Maskey, S., Van Gelder, P. H. A. J. & Vrijling, J. K. 2016 Comparison of empirical statistical methods for downscaling daily climate projections from CMIP5 GCMs: a case study of the Huai River Basin, China. *Int. J. Climatol.* **36** (1), 145–164.

Watanabe, M., Suzuki, T., O'ishi, R., Komuro, Y., Watanabe, S., Emori, S. & Takata, K. 2010 Improved climate simulation by MIROC5: mean states, variability, and climate sensitivity. *J. Clim.* **23** (23), 6312–6335.

First received 13 August 2018; accepted in revised form 9 December 2018. Available online 16 January 2019